J Biol Inorg Chem (2009) 14:1037–1052
DOI 10.1007/s00775-009-0547-z

ORIGINAL PAPER

DNA interactions and photocatalytic strand cleavage by artificial nucleases based on water-soluble gold(III) porphyrins

Martin Haeubl · Lorenz Michael Reith · Bernadette Gruber · Uwe Karner · Norbert Müller · Günther Knör · Wolfgang Schoefberger

Received: 16 February 2009 / Accepted: 4 May 2009 / Published online: 27 May 2009

Abstract The novel gold porphyrin complex (5,10,15-tris(*N*-methylpyridinium-4-yl)-20-(1-pyrenyl)-porphyrinato) gold(III) chloride, $[Au^{III}(TMPy_3Pyr_1P)](Cl)_4$, was prepared and characterized by optical spectroscopy, high-resolution nuclear magnetic resonance (NMR), and electrospray mass spectrometry. This cationic multichromophore compound exhibits excellent water solubility and does not form aggregates under physiological conditions. Binding interactions of this complex and related model compounds with nucleic acid substrates have been studied and characterized by NMR and circular dichroism spectroscopy. The photoreactivity of $[Au^{III}(TMPy_3Pyr_1P)](Cl)_4$ was investigated under anaerobic and aerobic conditions in the presence of an excess of purine nucleoside, guanosine, and plasmid DNA. Photocatalytic oxidative degradation of guanosine and the change from supercoiled to circular plasmid DNA upon monochromatic irradiation and polychromatic blue-light exposure with a maximum at 420 nm was explored. The potential of the novel water-soluble cationic metallo-intercalator complex $[Au^{III}(TMPy_3Pyr_1P)](Cl)_4$ to serve as a catalytic photonuclease for the cleavage of DNA has been demonstrated.

Keywords Cationic porphyrins · Gold · Pyrene · DNA · Metallointercalators

Introduction

At the borderlines of chemistry and biology there is an increasing interest in the design of synthetic reagents which are capable of performing specific biomimetic functions such as catalytic substrate conversion or regulatory processes under controlled conditions [1, 2]. Recently, in a review article, photochemical key steps were pointed out to be a versatile tool for achieving these goals [3]. Chemical nuclease mimics have been among the first successful examples of compounds with artificial enzyme function driven by light [4, 5]. While these systems are considered to have many potential uses as tools in molecular biology or as therapeutic agents for molecular photomedicine and photodynamic cancer treatment, there is still a significant lack of artificial nucleases displaying catalytic turnover in the transformation of DNA or RNA substrates. Double-strand scission of DNA, which mimics the function of natural restriction enzymes, requires two nucleic acid cleavage steps in close proximity without release, consumption, or deactivation of the reagent involved. This may be achieved via compounds composed of two

Electronic supplementary material The online version of this article (doi:10.1007/s00775-009-0547-z) contains supplementary material, which is available to authorized users.

M. Haeubl · L. M. Reith · B. Gruber · N. Müller
Institut für Organische Chemie,
Johannes Kepler Universität Linz (JKU),
Altenberger Str. 69, 4040 Linz, Austria

G. Knör (✉) · W. Schoefberger (✉)
Institut Für Anorganische Chemie,
Johannes Kepler Universität Linz (JKU),
Altenberger Str. 69, 4040 Linz, Austria
e-mail: guenther.knoer@jku.at

W. Schoefberger
e-mail: wolfgang.schoefberger@jku.at

U. Karner
Institut für Chemische Technologie Organischer Stoffe,
Johannes Kepler Universität Linz (JKU),
Altenberger Str. 69, 4040 Linz, Austria

functional subunits tethered by a flexible covalent linker or by cleaving reagents with high catalytic efficiency and turnover numbers.

In the present work, we selected photoreactive gold porphyrins with additional nucleic acid targeting groups as potential candidates for the development of catalytic photonucleases. These compounds were selected for the following reasons. The presence of a high-valent central atom and the combination with weakly coupled chromophore subunits in the ligand periphery introduces additional excited states of the charge-transfer type, which are known to determine the photophysical and photochemical behavior of gold porphyrins [6–8] These unique properties are expected to be beneficial for the desired photonuclease activity. In previous work, the efficient catalytic transformation (turnover number 700) of the nucleobase guanine was demonstrated with a pyrene-functionalized gold(III) porphyrin complex, which, however, showed unsatisfactory solubility properties [7, 9]. An overall polycationic charge was now introduced into such systems, which should facilitate water solubility and targeting toward the polyanionic phosphate backbone of nucleic acids under physiological conditions. Furthermore, gold(III) metalloporphyrins are usually among the most powerful electron acceptors in the series of tetrapyrrole-based photosensitizers, and thus act as strong photooxidants.

Oxidative damage of DNA plays a critical role in mutagenesis, carcinogenesis, aging, and lethality [10–12]. DNA can be oxidized by reactive oxygen species, ionizing radiation, and transition metal complexes. These oxidation reactions may induce modifications within the sugar or base moieties of DNA, leading to strand scission or base modification. Many transition metal complexes, including those of vanadium, chromium, manganese, rhenium, ruthenium, osmium, cobalt, rhodium, nickel, palladium, and copper, have been studied as potential probes of nucleic acid structure and for potential applications as drugs [13–17] which mediate DNA oxidation in the presence of ionizing radiation, photosensitizers, or oxidants. In the presence of O_2, H_2O_2, or SO_3^{2-}, complexes containing Cr^{VI}, Mn^{II}, Fe^{III},Co^{II}, Ni^{II}, or Cu^{II} may generate radicals that can abstract one electron from guanine. Iron(II) bleomycin, iron(II) EDTA/H_2O_2, and photoexcited charge-transfer complexes (Ru^{III}) modify DNA by direct strand scission [13–15].

High-valent oxo-metal ($Mn^{V}\equiv O$, Ru^{IV}=O, Os^{IV}=O, Cr^{V}=O) complexes oxidize DNA at both sugar and base sites. The oxo-manganese(V) porphyrin formed from $[Mn(III)(TMPyP)]^{5+}$/$KHSO_5$ = Mn(III) *meso* tetrakis(*N*-methylpyridinium-4yl) porphyrin pentachloride (activated with $KHSO_5$) abstracts two electrons from guanine to produce the guanine cation, G^{+}. The major oxidation product (more than 90%) from monomeric G is 2-amino-5-[(2-deoxy-*β*-D-*erythro*-pentofuranosyl)amino]-4*H*-imidazol-4-one (imidazolone), but several other oxidation products are formed from double-stranded oligonucleotides [18]. Oxidation of a dinucleoside monophosphate d(GpT) by $Mn^{V}\equiv O$, proposed to follow a net two-electron mechanism, produces dehydroguanidinohydantoin as a major oxidation product [19]. Ru^{III} complexes coordinate to N7 of deoxyguanosine [20] and inosine [21] and facilitate autoxidation of the nucleosides to yield the corresponding 8-ketonucleosides. Ru^{IV}=O complexes oxidize guanine via an inner-sphere atom transfer to produce 7,8-dihydro-8-oxo-guanine (8-oxo-G) [22–25]. High-valent nickel complexes (Ni^{III}) formed from NiCr/$KHSO_5$ bind to N7 of G and react by a one-electron mechanism [26, 27]. Cr^{V}=O complexes initiate DNA cleavage through a chromium(V) phosphate diester intermediate by hydrogen abstraction from C1′.

Some transition metal species such as Ir^{IV}, MnO_4^{2-}, Os^{III}, and Ru^{III} are reported to further oxidize 8-oxo-G [28], a major oxidation product of guanine in double-stranded DNA. Platinum coordination compounds are biologically important for their anticancer activity [10]. Pt^{II} complexes bind preferentially to the N7 position of G [29]. Cisplatin, *cis*-diamminedichloroplatinum(II), binds bifunctionally to adjacent Gs and kinks DNA [30]. High mobility group proteins and p53 protein bind to the platinum-modified DNA, preventing DNA replication, and leading to cell death [31]. Some Pt^{IV} complexes have shown potential as powerful anticancer drugs, although most Pt^{IV} anticancer drugs have been considered to be Pt^{II} prodrugs [32]. Since Pt^{IV} complexes are kinetically inert [33], reaction with DNA is not expected until they have been reduced to Pt^{II} in the cellular medium [12]. However, direct Pt^{IV} binding to DNA has been observed in vitro in several laboratories [34–36]. Choi et al. [37] reported that Pt^{IV} complexes with highly electron withdrawing and bulky ligands have high reduction potentials and high reactivity toward the monomeric nucleotide GMP [38]. Furthermore, $[Pt^{IV}Cl_4(dach)]$ (dach = 1,2-cyclohexanediammine), which has a high redox potential, oxidizes guanine in GMP, 2′-deoxyguanosine 5′-monophosphate (dGMP), 2′-deoxyguanosine, 2′-deoxyguanylyl-(3′-5′)-2′-deoxyguanosine, and a double-stranded oligonucleotide without any UV radiation or additional oxidants [39]. The major oxidation product was identified as 8-oxo-G. Choi et al. observed that [Pt(IV)Cl_4(dach)] further oxidizes 8-oxo-G and proposed a mechanism involving the Pt(IV) binding to N7 of dGMP followed by cyclization via nucleophilic attack of phosphate oxygen at C8 of dGMP. The next step is an inner-sphere, two-electron transfer to produce a cyclic phosphodiester intermediate, 8-hydroxyguanosine cyclic 5′,8-hydrogen phosphate. This intermediate slowly converts to 8-oxo-dGMP by reacting with solvent H_2O.

Gold(III) compounds

The Au^{III} coordination center is isoelectronic with Pt^{II} and both give rise to square-planar geometries; the main difference between gold(III) and platinum(II) compounds is that ligand substitution reactions are usually much faster in the case of gold(III) compounds [40]. The high analogy to platinum(II) compounds makes gold(III) complexes good candidates for development and testing as anticancer drugs, although the relatively low kinetic stability and the usually high redox potentials have largely hampered such investigations. Some recent studies reporting that novel gold(III) compounds show favorable antitumor properties both in vitro and in vivo have raised new interest in this class of complexes [41]. The few gold(III) compounds for which advanced pharmacological testing has been carried out offer a rather puzzling mechanistic profile. Gold(III) porphyrin complexes show direct DNA damage; in the other cases the effects on DNA and on the cell cycle appear to be modest, so it is rather unlikely that DNA may represent the ultimate target. Gabbiani et al. [42] have shown that cytotoxicity caused by the gold(III) complexes $[Au(phen)Cl_2]Cl$ and $[Au(dien)Cl]Cl_2$ (phen = phenanthroline and dien = diethylenetriamine) only results in very marginal DNA damage; additionally only weak cell cycle effects were seen in comparison with cisplatin, further suggesting a different molecular mechanism. A similar situation was previously found for gold(III) DAMP = (2-[(dimethylamino)methyl] phenyl) compounds exhibiting modest DNA binding properties [41]. Thus, DNA is likely not to be the primary target for several of the gold(III) compounds investigated. Even in the cases where some evidence of a direct interaction with DNA has been reported, e.g., the gold(III) porphyrin complexes, the mechanisms of DNA damage and cell death appear to be distinct from those induced by platinum metallodrugs. On the basis of newly obtained experimental evidence it is tempting to propose that gold(III) compounds may exert their cytotoxic effects by causing direct mitochondrial damage through modification of specific proteins. Recently, a study conducted by the groups of Bindoli, Rigobello, and Messori, who observed that a few gold(III) complexes are tight inhibitors of the selenoenzyme thioredoxin reductase, a crucial enzyme for protecting the cell against oxidative stress. Accordingly, these compounds were found to perturb greatly the mitochondrial functions [42–47]. This hypothesis is further reinforced by the observation that antiarthritic gold(I) compounds such as auranofin are known as potent inhibitors of thioredoxin reductase and as effective antimitochondrial agents [47–49].

Nevertheless, DNA is one of the major targets for anticancer drugs [50] and binding of metalloporphyrins to DNA has been studied extensively [51]. Che et al. [45] examined the interaction of gold(III) porphyrins with duplex DNA by UV–vis absorption titrations. Isosbestic spectral changes and significant hypochromicity of the Soret band were noticed upon addition of calf thymus DNA (CT-DNA), suggesting a direct interaction of gold(III) porphyrins with the DNA double helix. Moreover, by using confocal microscopy, the authors reported that gold(III) porphyrins induce extensive apoptosis in HeLa cancer cells. In addition to morphological changes, fragmentation of genomic DNA was also observed after incubating the HeLa cells with Au(III) *meso* tetraphenylporphyrin (Au(TPP)) for 15 h [52, 53].

On the molecular basis of DNA fragmentation, the heterocyclic bases are reactive and it is generally accepted that the purine base guanine (G) is the site of lowest ionization potential in DNA. Acting as a hole trap in long-range electron transfer reactions, guanine is oxidized to the intermediate cationic radical $G^{\cdot+}$, which gives rise to the permanent lesions that enable a sequence of specific DNA strand scission. Photoinduced formation of guanine radical cations and the development of synthetic nucleic acid cleavage agents which can be controlled by light (photonucleases) are therefore active areas of research.

In this context, we designed a novel water soluble gold(III) porphyrin (5,10,15-tris(*N*-methylpyridinium-4-yl)-20-(1-pyrenyl)porphyrinato)gold(III) chloride, $[Au^{III}(TMPy_3Pyr_1P)](Cl)_4$ (**4**), as a potential new cytotoxic photosensitizer, which combines the high DNA binding affinity of cationic polycyclic aromatic hydrocarbons with the prodrug properties of gold-based chemotherapeutic agents [45, 54–56]. The present paper describes the synthesis and characterization of **4** and degradation reactions of DNA, dGMP and guanosine induced by this complex. The mechanistic differences between **4** and the nonmetalated porphyrin 5,10,15-tris(*N*-methylpyridinium-4-yl)-20-(1-pyrenyl)-21*H*,23*H*-porphyrin chloride, $H_2(TMPy_3Pyr_1P)(Cl)_3$ (**3**), were determined using electrospray ionization (ESI)–time of flight (TOF) spectrometric and NMR spectroscopic methods.

Results

Synthesis and electronic spectra

We synthesized the highly water soluble **4** by the procedures described in "Materials and methods" (Fig. 1).

Figure 2 shows typical electronic absorption spectra of the free-base ligand **3** and the gold complex **4**. The absorption maximum at 423 nm corresponds to the Soret, or B, band of **3**. The free-base porphyrin displays the typical pattern of four Q bands in the visible spectral region, showing a phyllo-type intensity distribution. A further, rather sharp absorption feature is present in the

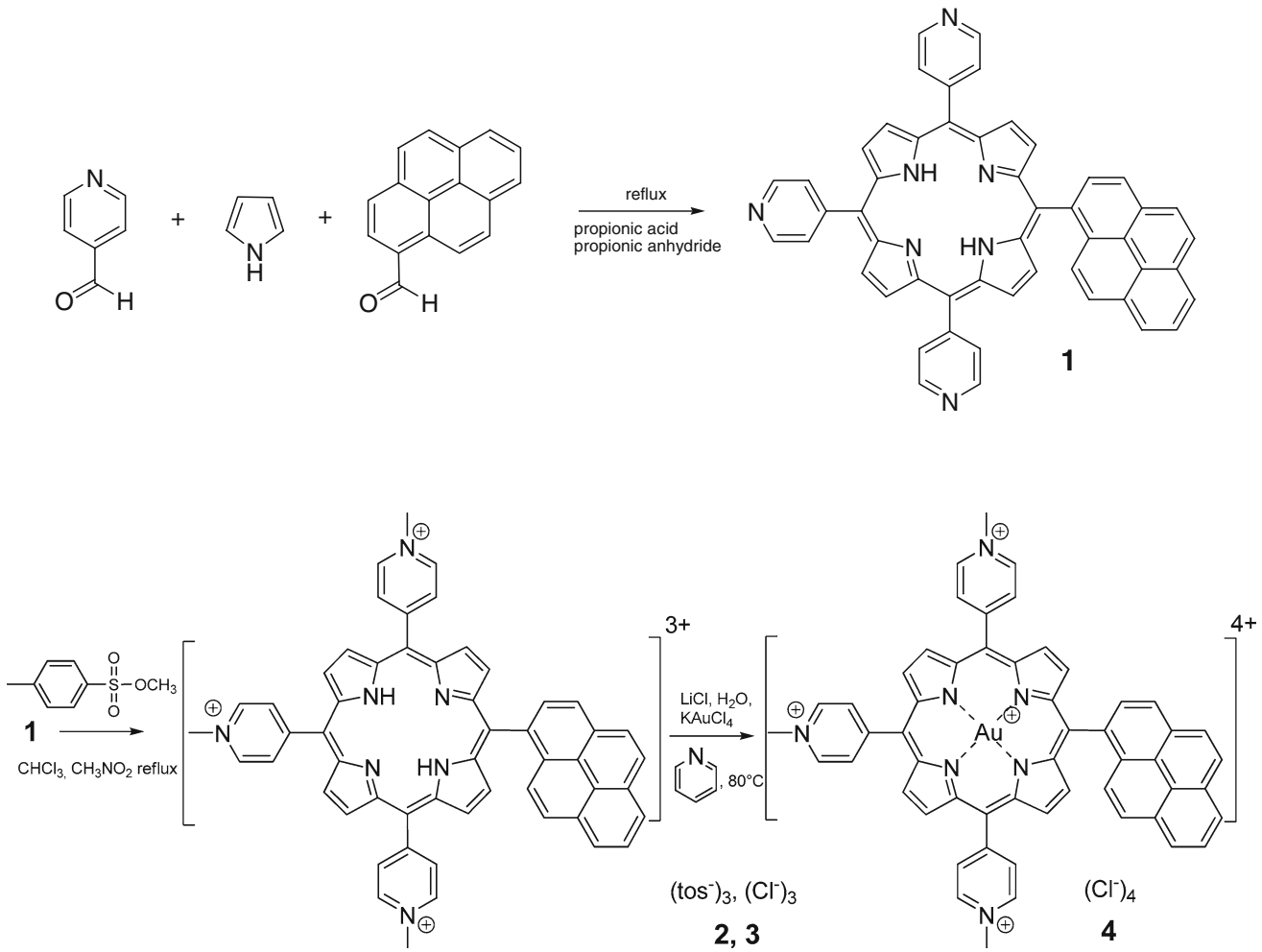

Fig. 1 Structures of $H_2(TPy_3Pyr_1P)$ (**1**), $H_2(TMPy_3Pyr_1P)(tos)_3$ (**2**), $H_2(TMPy_3Pyr_1P)(Cl)_3$ (**3**), and $[Au^{III}(TMPy_3Pyr_1P)](Cl)_4$ (**4**)

300–350-nm spectral region, which can be attributed to allowed intraligand transitions involving the π-electron system of the 1-pyrenyl substituent. Only a weak electronic coupling of the porphyrin and pyrenyl chromophore subunits occurs in the ground state. Metalation of **3** with potassium tetrachloroaurate(III) gives rise to a significant blueshift of the Soret maximum of **4** to 408 nm, which is characteristic for the complexation of porphyrins with gold(III) or other transition metals such as platinum(II) with *d*-electron configurations resulting in so-called irregular hypso-type electronic spectra. The position of the pyrenyl absorption is unaffected by the metalation, which is in agreement with the interpretation of **3** as a weakly coupled multichromophore ligand. As has been observed before with related systems such as the tetrapyrenylporphyrin complex 5,10,15,20-tetrakis(1-pyrenyl) porphyrinato)gold(III) acetate an additional intraligand charge-transfer absorption feature is present in the visible spectral region around 430–460 nm (Fig. 2) [7].

Luminescence and excited state lifetime measurements

Emission spectra of the gold porphyrin complex **4** were studied in a low-temperature matrix to determine the electronic origin of the lowest-lying excited states, which is an important prerequisite to estimating excited-state redox potentials [51]. In Fig. 2, the excitation and luminescence data for the compound measured in ethanol at 77 K are presented. The metalloporphyrin exhibits a structured emission band in the red and near-IR spectral region with a luminescence maximum at 684 nm. The excitation spectrum for this peak matches very well the absorption spectrum of the metal complex. In agreement with previously reported data on other gold(III) porphyrins [52], the luminescence spectrum observed is assumed to be a phosphorescence originating from the triplet-state manifold of **4**. The triplet energy of the photosensitizer is obtained with reasonable precision from the 0–0 band of the phosphorescence spectrum at 77 K, which approximately coincides

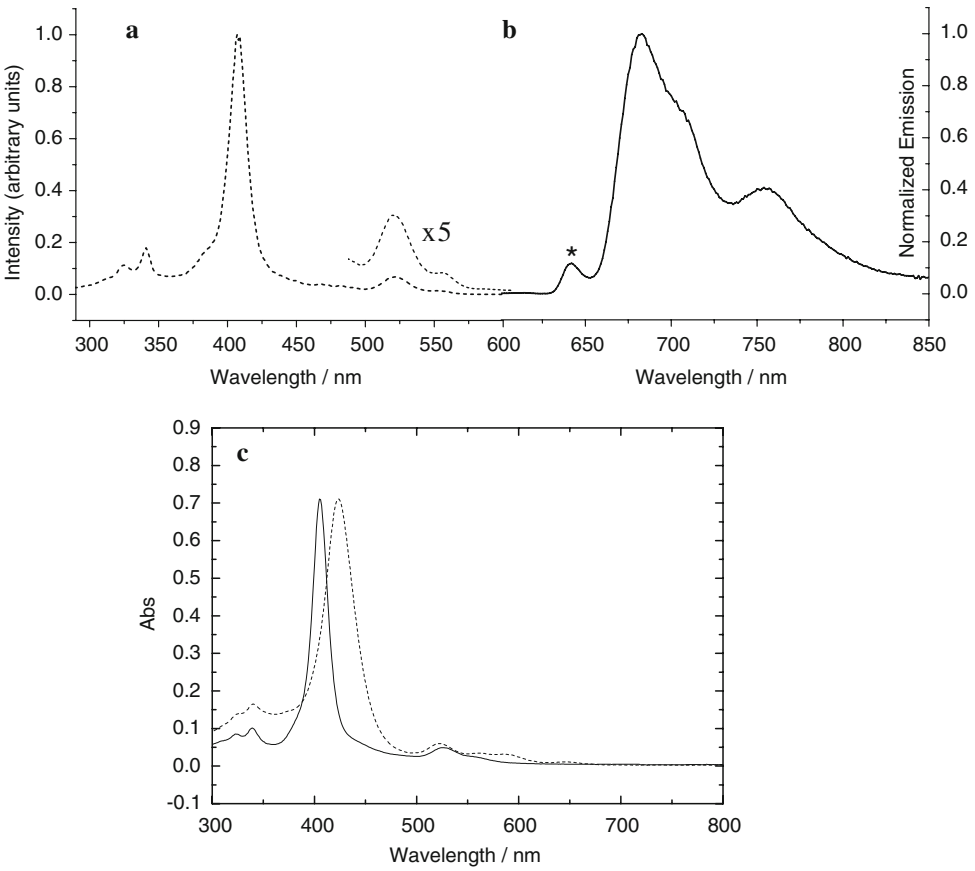

Fig. 2 *a* $[Au^{III}(TMPy_3Pyr_1P)](Cl)_4$ luminescence excitation spectrum detected at 684 nm (*left*) and *b* emission spectrum (*right*) for excitation at 408 nm at 77 K in an ethanol matrix. The small peak around 650 nm, marked with an *asterisk*, corresponds to the presence of trace amounts of free-base porphyrin, which displays its fluorescence maximum at this wavelength. *c* UV–vis absorption spectrum of the free-base porphyrin $H_2(TMPy_3Pyr_1P)(Cl)_3$ (*dotted line*) and its gold complex $[Au^{III}(TMPy_3Pyr_1P)](Cl)_4$ (*solid line*) in 5 mM sodium cacodylate buffer (20 mM NaCl, pH 7.0) at 298 K

with the short-wavelength peak maximum at 684 nm, corresponding to an energy value of 14,600 cm^{-1}, or $E_T = 1.8$ eV.

Phosphorescence decay measurements at low temperatures show a monoexponential deactivation with a single lifetime of about 130 μs at 77 K (Fig. S9) for **4**. This value fits very well to the long-lived component of the multiexponential decay reported by Eng et al. [57], who presented a detailed triplet photophysics study for the gold porphyrin AuT(DtBP)P = gold(III)5,10,15,20-tetra(3,5-di-tert-butylphenyl)- porphyrin in PMMA = (poly(methyl)methacrylate) and EPA = (diethyl ether/isopentane/ethanol (5:5:2)) at various temperatures. The more complex photophysics observed with this latter porphyrin and several other gold porphyrins is due to a strong interference of an additional ligand-to-metal charge-transfer (LMCT) state in the energetic range of the porphyrin triplet manifold. In the case of **4**, the situation tends to become less complicated, since the LMCT state is expected to be shifted to higher energy (the macrocyclic ring is more difficult to oxidize) owing to the presence of multiple positive charges at the porphyrin ligand. Further detailed studies, however, are necessary to test this hypothesis, even though all preliminary electrochemical data collected up to now (see later) seem to confirm this assumption.

Cyclic voltammetry

Electrochemical measurements were carried out to quantify the oxidation power of **4** when acting as an electron acceptor in reductive excited state quenching processes and electron transfer mediated DNA damage. In cyclic voltammetry experiments (see Fig. S10), as expected for a gold(III) porphyrin complex, the compound displays several consecutive reduction waves at rather positive potentials, which in principle may involve the porphyrin ring, the central metal cation, and the peripheral substituents, especially the pyridinium cation subunits [52–54]. In our case, the first and the second reductions show a peak-to-peak separation of about 60 mV and a reverse peak to forward peak current ratio close to unity, suggesting that both electrode processes are reversible and involve the transfer of one electron. The first fully reversible reduction occurs at a potential of $E_{1/2}(\mathbf{4}/\mathbf{4}^-) = -0.51$ V versus the internal ferrocene/ferrocenium standard [corresponding to about +0.13 V vs. the normal hydrogen electrode (NHE)]. Taking into account the triplet energy of $E_T = 1.8$ eV obtained in our phosphorescence studies, we can estimate an excited-state redox potential of +1.29 V versus ferrocene/ferrocenium (+1.93 V vs. NHE) [51] for photoinduced one-electron transfer processes of **4**. This value, as

expected, is among the highest oxidation potentials observed in the family of metalloporphyrin photosensitizers. Therefore, the direct photoinduced oxidation of nucleobases such as guanine (+1.29 V vs. NHE) [5] is clearly thermodynamically possible.

At present, the site of the first reduction of **4** remains unclear and will be unambiguously explored by means of spectroelectrochemistry in our further studies. Recent work by Kadish et al. [58] has shown that in some gold(III) porphyrins the first reduction actually may take place at the metal center rather than at the macrocyclic ligand. In such systems, the LMCT excited states involving the gold center may occur at rather low energies, thus leading to rather complicated photophysical properties as described above. In our case, however, consistent with the photophysical results, the presence of the cationic pyridyl groups is expected to shift the first porphyrin-ring-centered reductions to rater low reduction potentials and the electrochemical reduction will first involve the porphyrin-based lowest unoccupied molecular orbitals instead of the empty gold(III) $d_{x^2-y^2}$ orbital [52]. The one-electron reduction product formed at −0.51 V versus ferrocene/ferrocenium will then be best described with metalloporphyrin radical anion characteristics.

Interaction and stability of DNA/porphyrin complexes

Circular dichroism (CD) spectroscopy was applied to study the interaction modes of DNA with the synthesized gold porphyrin complex (**4**). Double-stranded B-DNA d(GCGCGC)$_2$ and A-DNA d(ATATAT)$_2$ was added to a solution of **4**. In Fig. 3 the CD spectra of the commercially available 5,10,15,20-tetrakis(*N*-methylpyridinium-4-yl-porphyrin) chloride, H_2(TMPyP)(Cl)$_4$, and our new asymmetric porphyrin derivatives **3** and **4** interacting with B-DNA and A-DNA are compared.

According to Guliaev and Leontis [59] and Kim et al. [60], H_2(TMPy$_4$P)(Cl)$_4$ shows intercalation to the B-DNA hexamer d(GCGCGC)$_2$ and outside binding to A-DNA d(ATATAT)$_2$. The nonmetalated multichromophore porphyrin **3** follows the findings of Guliaev and Leontis and Kim et al. and indicates outside binding with self-stacking to the AT oligomer (Fig. 3, spectrum c), whereas intercalation occurs to GC-rich regions (Fig. 3, spectrum d). The additional peak at 350 nm in Fig. 3, spectrum c also indicates another binding mode, where the pyrenyl moiety of compound **3** is involved in the binding with A-DNA. This peak was not observed in the complex with B-DNA.

The gold porphyrin derivative **4** shows interaction to both GC- and AT-rich regions of DNA (Fig. 3, spectra a, b). According to Pasternack and Gibbs [61], the overlying positive and negative peaks in Fig. 3, spectra a, c, and e indicate outside binding with self-stacking to the DNA duplexes [61–63]. CT-DNA melting points were determined

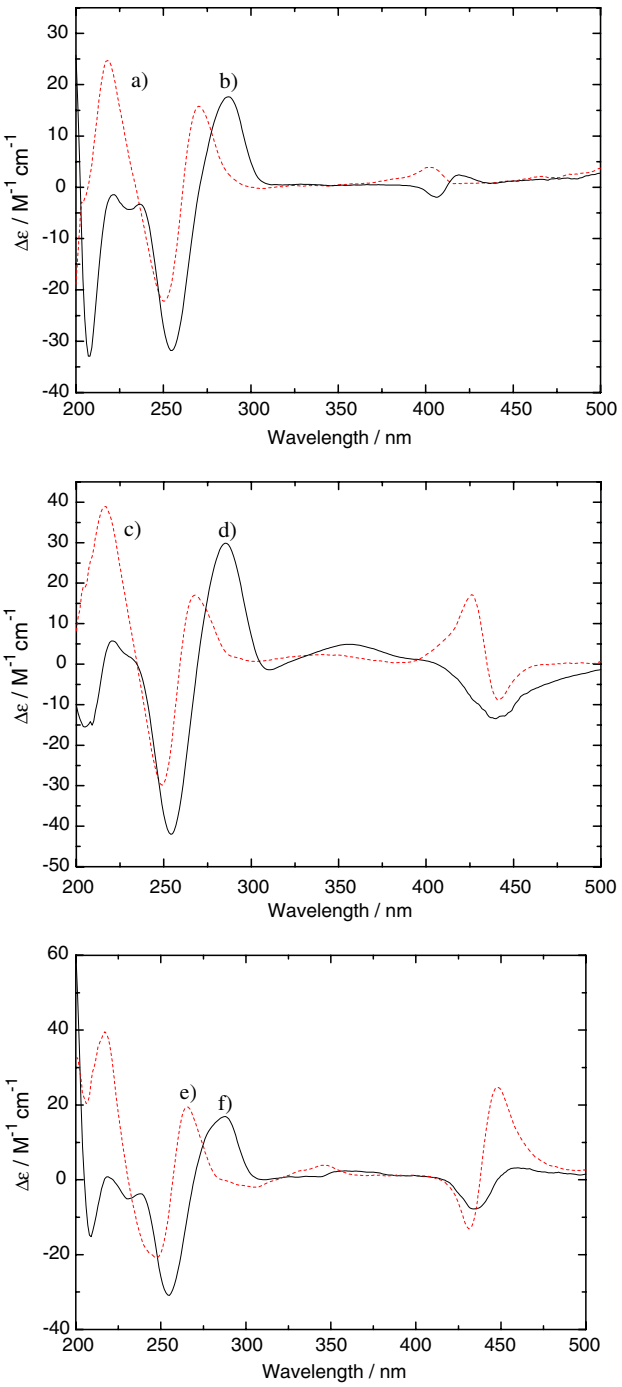

Fig. 3 Circular dichroism spectra of the porphyrin/DNA oligonucleotide complexes *a* [Au^{III}(TMPy$_3$Pyr$_1$P)](Cl)$_4$/d(ATATAT)$_2$, *b* [Au^{III}(TMPy$_3$Pyr$_1$P)](Cl)$_4$/d(GCGCGC)$_2$, *c* H_2(TMPyP)(Cl)$_4$/d(ATATAT)$_2$, *d* H_2(TMPyP)(Cl)$_4$/d(GCGCGC)$_2$, *e* H_2(TMPy$_3$Pyr$_1$P)(Cl)$_3$/d(ATATAT)$_2$, and *f* H_2(TMPy$_3$Pyr$_1$P)(Cl)$_3$/d(GCGCGC)$_2$ all in equimolar solutions (0.2 mM DNA, 0.2 mM porphyrin) in 5 mM sodium cacodylate, 20 mM NaCl pH 7.0 buffer [d(GCGCGC)$_2$ at 293 K, d(ATATAT)$_2$ at 277 K]

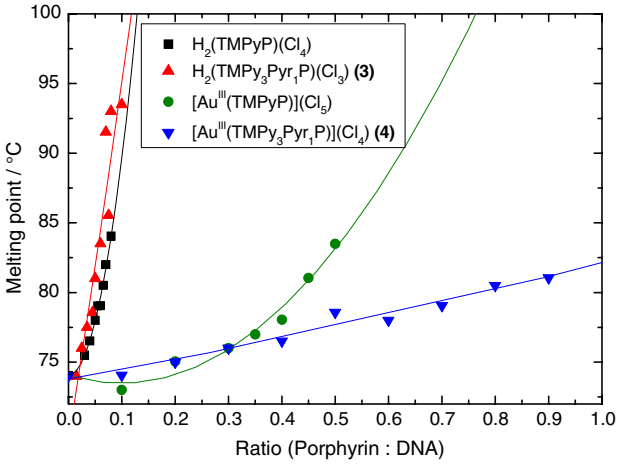

Fig. 4 Calf thymus DNA melting point experiments for $H_2(TMPyP)(Cl)_4$, $[Au^{III}(TMPyP)](Cl)_5$, $H_2(TMPy_3Pyr_1P)(Cl)_3$, and $[Au^{III}(TMPy_3Pyr_1P)](Cl)_4$; 0.06 mM calf thymus DNA, 5 mM sodium cacodylate, 20 mM NaCl at pH 7.0

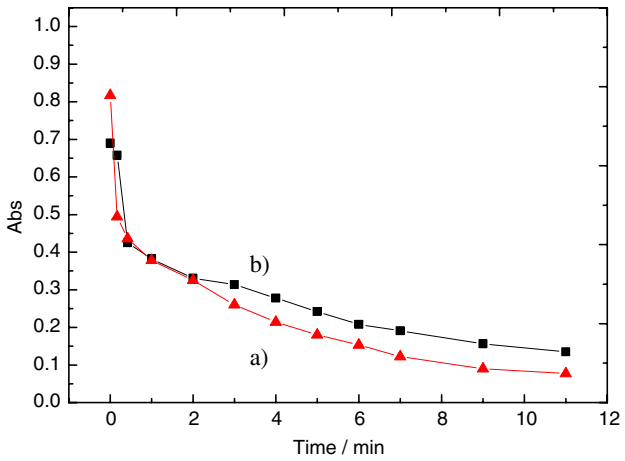

Fig. 5 Photosensitized generation of singlet oxygen versus time by *a* rose Bengal and *b* $[Au^{III}(TMPy_3Pyr_1P)](Cl)_4$ using a 1,3-diphenylisobenzofurane (DPBF) assay with *a* 0.05 μM rose Bengal and *b* 0.03 mM $[Au^{III}(TMPy_3Pyr_1P)](Cl)_4$ and 0.17 mM DPBF in ethanol, 298 K

to assess the stabilization of double-stranded DNA by the drug candidates. The DNA was exposed to **4**. Figure 4 shows a comparison of the changes in DNA melting points induced by four different porphyrin derivatives. The interaction of the nonmetalated **3** and the well-known, commercially available, $H_2(TMPyP)(Cl)_4$ cause higher DNA melting points than the corresponding gold compounds. At a ratio of 1:10 (porphyrin to DNA), melting points with the gold porphyrins are 273 K lower than for mixtures with the corresponding nonmetalated porphyrins. From these findings a lower stabilization of the DNA/gold porphyrin complexes compared with the DNA/free-base porphyrin complexes can be deduced.

Photogeneration of singlet oxygen

A standard assay based on 1,3-diphenylisobenzofurane (DBPF) was applied to follow the well-established singlet oxygen generation by the reference sensitizer rose Bengal. As shown in Fig. 5, the formation of $^1O_2$ was also sensitized by **4** when an air-saturated solution was irradiated. In the presence of DBPF as a trap, both photosensitizers display comparable rates of $^1O_2$ formation. The profiles of the curves suggest a rapid consumption of the dissolved dioxygen in the teflon-stoppered cuvettes used.

Oxidation of guanosine and 5′-dGMP

5′-dGMP oxidation under aerobic and anaerobic conditions

The decreases in UV absorption of guanosine at 270 nm in the presence of **4** upon irradiation at 420 nm both under aerobic and anaerobic conditions are shown in Fig. 6a and b, respectively. Incubation of all relevant nucleoside 5′-monophosphates (5′-dAMP, 5′-dGMP, 5′-dTMP, 5′-dCMP) with **4** was carried out independently and monitored by NMR spectroscopy and ESI quadrupole TOF (Q-TOF) mass spectrometry. No reactions were observed in the cases of dCMP, dAMP, and dTMP, while during incubation of **4** with 5′-dGMP a reaction was observed. The main compound was identified as the nonreacted substrate dGMP radical by the $(M - 1)^{\cdot -}$ anion peak at $m/z = 346$. The base peak at 378 m/z corresponds to the $(M + 32)^{\cdot -}$ radical anion of an oxidation product (dGMP + O_2). Corresponding to the singlet oxygen formation described above, we assume a reaction mechanism over an endoperoxide intermediate reacting to give 5-hydroxy-8-oxo-2′,2′′-deoxyguanosine 5′-monophosphate (5-HO-8-oxo-dGMP) (**6**) according to the reaction scheme in Fig. 7 [64, 65]. The anion peak at 266 m/z belongs to the $[8\text{-oxo-dGMP}]^{\cdot -}$ radical anion (**5**) ($C_{10}H_{12}N_5O_4^{\cdot -}$) after the loss of the phosphate group. The deprotonated 8-oxo-G ($C_5H_3N_5O_2^{\cdot -}$) radical anion causes the peak at 165 m/z, and the fragment at 150 m/z is assigned to the guanine radical anion ($C_5H_4N_5O^{\cdot -}$).

^1H NMR spectroscopy corroborates the proposed structures by the observation of the shifted signals in the sugar proton region H2′, H3′, H4′, and H5′ (4.4–3.5 ppm, Fig. 8a). Additionally, a new shifted H1′ triplet signal arises during irradiation (Fig. 8b). Double quantum filtered correlation spectroscopy (DQF-COSY) and ^1H–^{13}C heteronuclear multiple bond correlation (HMBC) NMR spectra of the photoinduced reaction mixture confirm the degradation product structures 8-oxo-dGMP and 7,8-dihydro-4-hydroxy-8-oxo-2′-deoxyguanosine 5′-monophosphate leading to the spiroiminohydantoin as the end product of

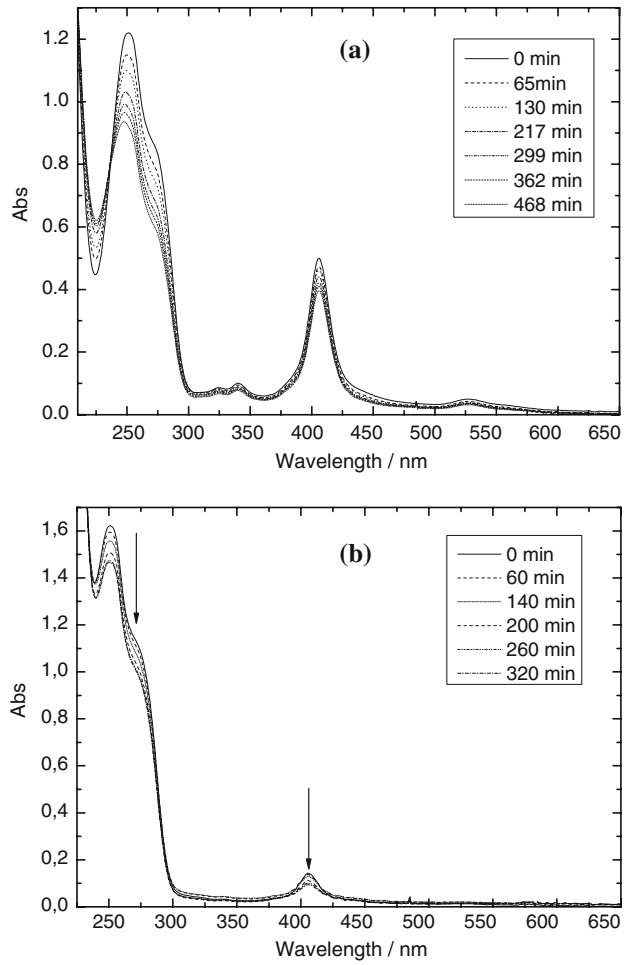

Fig. 6 Guanosine degradation upon monochromatic excitation at 420 nm. UV–vis spectral changes **a** under aerobic conditions and **b** under anaerobic conditions with 0.08 mM guanosine, 0.05 mM $[Au^{III}(TMPy_3Pyr_1P)](Cl)_4$ in 5 mM sodium phosphate, 75 mM NaCl pH 7.0 buffer

the photoinduced reaction under aerobic conditions. The ^{31}P NMR spectra in Fig. 9 corroborate the degradation of 5′-dGMP through the appearance of a new site at 3.15 ppm (indicated by an asterisk) and a shift of the main peak from 3.20 to 2.50 ppm.

The same reaction was performed under anaerobic conditions, where the abstraction of one electron from (G-H) apparently produces a radical cationic species $(8\text{-oxo-dGMP})^+$. The attack of a water molecule is possible on $(8\text{-oxo-dGMP})^+$, a reaction which is also referred to as hydration of the radical cation [66]. After deprotonation of the adduct, this route produces a neutral radical species (5-hydroxy-8-oxo-2,2′-deoxyguanosine 5′-monophosphate; 5-OH-8-oxo-dGMP), which can be further oxidized by a second electron abstraction to generate the 5-OH-8-oxo-G. This intermediate collapses into guanidinohydantoin 2′-deoxyribonucleotide 5′-monophosphate (**7**) and spiroiminodihydantoin 2′-deoxyribonucleotide 5′-monophosphate (**8**) as shown in Fig. 10 [67]. The products Gh and Sp were detected by ESI-Q-TOF mass spectrometry. The ion peak at 352.066 *m/z* can be assigned as the **7** radical anion ($C_9H_{15}N_5O_8^{-}$). The peak at 255.23 *m/z* indicates the fragmentation product of **7** ($C_{10}H_{13}N_5O_5^{-}$) due to the loss of the phosphate group. The base peak at 378 *m/z* corresponds to the deprotonated ion of the oxidation product **8** $[M - 1]^-$. The peak at 281.27 *m/z* corresponds to fragmentation of **8** $[M - 97]^{\cdot -}$, involving the loss of the phosphate unit. The peak at 266 *m/z* corresponds to the radical anion ($C_{10}H_{12}N_5O_4^{\cdot -}$), indicating the fragmentation of 8-oxo-dGMP (**5**), which may come from traces of oxygen owing to incomplete degassing of the reaction mixture.

The degradation product was assigned from ^1H–^{13}C heteronuclear single quantum coherence (HSQC), ^1H–^{13}C HMBC, and ^1H–^1H DQF-COSY NMR spectra (Figs. S4–

Fig. 7 Oxidation of 5′-dGMP with $[Au^{III}(TMPy_3Pyr_1P)](Cl)_4$ during irradiation at 420 nm. The anaerobic reaction is initiated at the 4′ carbon by a radical formation due to hydrogen abstraction

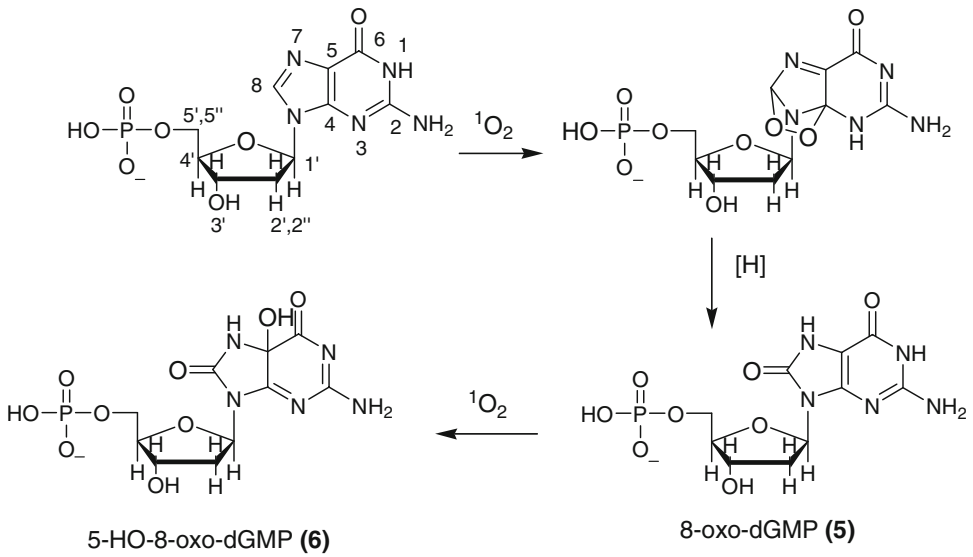

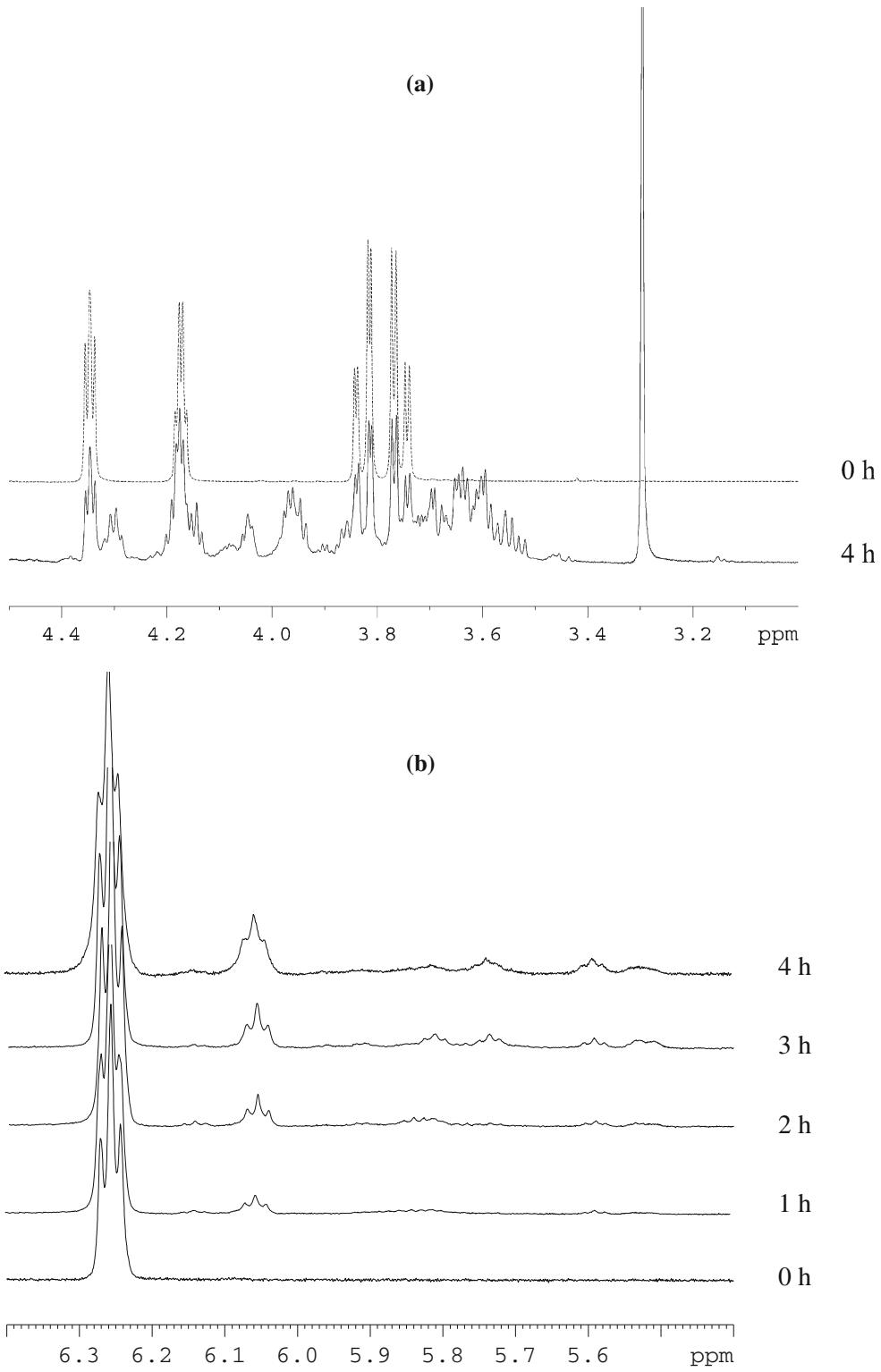

Fig. 8 **a** ^{1}H NMR spectra of the reaction of $[Au^{III}(TMPy_3Pyr_1P)](Cl)_4$ with 5′-dGMP at pH 7.5 and 310 K (H1′ region). **b** ^{1}H NMR spectra of the reaction of $[Au^{III}(TMPy_3Pyr_1P)](Cl)_4$ with 5′-dGMP (H8 region). 10 μM $[Au^{III}(TMPy_3Pyr_1P)](Cl)_4$, 4.9 mM 5′-dGMP in 99% D_2O (NMR: 303 K)

S7), and the assignment of **8** is summarized in Table S1. A further degradation product was observed via ^{1}H–^{13}C HSQC and the spectra indicated by a ^{1}H–^{13}C correlation at 5.53 ppm in the proton dimension and 100.0 ppm in the carbon dimension. The corresponding ^{1}H–^{13}C HMBC NMR experiment indicates correlation to the carbohydrate atoms C4′; C3, and C2′ and suggests an attack of hydroxyl groups at C5′. As a consequence of that, we assume that ·OH radicals react with the carbohydrate moiety of 5′-dGMP.

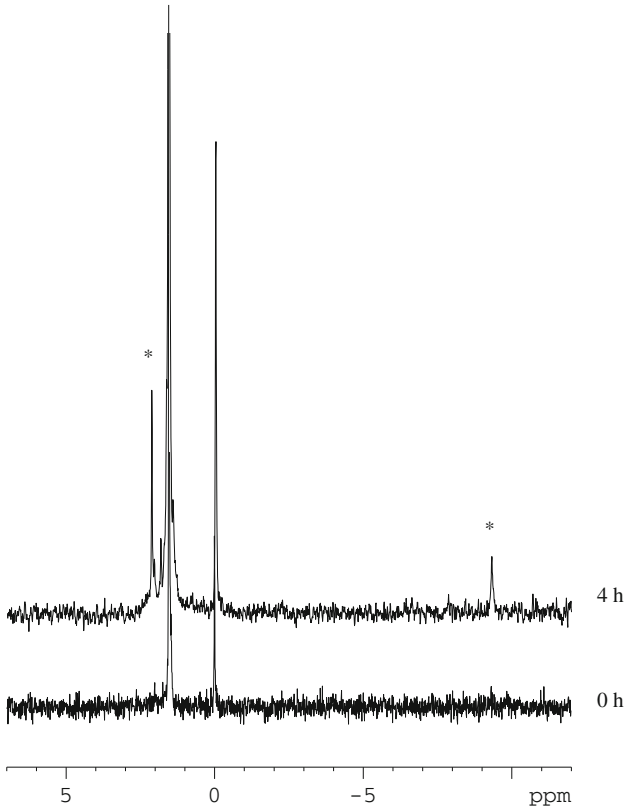

Fig. 9 ^{31}P NMR spectra of $[Au^{III}(TMPy_3Pyr_1P)](Cl)_4$ with 5′-dGMP at pH 7.5 and 308 K at irradiation times up to 4 h and an irradiation wavelength of 420 nm under aerobic conditions. 10 μM $[Au^{III}(TMPy_3Pyr_1P)](Cl)_4$, 4.9 mM 5′-dGMP in 99% D_2O (NMR: 303 K)

DNA cleavage experiments

The ^{31}P NMR spectra shown in Fig. 11 clearly show that cleavage of B-DNA $d(GCGCGC)_2$ is caused by the photosensitizer **4**. Without irradiation, well-resolved peaks of the phosphorous backbone residues (−1.0 to −1.5 ppm) can be seen. After irradiation for 2 h, a new phosphorous site at −0.1 ppm emerges, which might indicate that phosphate groups at the ends of the double strand are cleaved from the sugar. Next to this the clearly resolved region between −1.0 and −1.5 ppm loses resolution because new phosphorous sites are generated by the degradation process and the different lengths of the resulting oligonucleotide fragments.

Cleavage of supercoiled pBR322 DNA by **4** under irradiation at 420 nm in a Rayonet reactor was investigated using agarose gel electrophoresis. All experiments were performed in 5 mM sodium phosphate, 75 mM NaCl pH 7.0 buffer. The results of DNA cleavage for **4** are illustrated in Fig. 12. Control experiments indicated that no cleavage of DNA happened in the presence of **4** without illumination (lane c). The conversion of supercoiled DNA to nicked circular and linear duplex DNA at a concentration of 0.32 mM **4** under irradiation are shown in lanes d–k. With longer irradiation times the concentration of linear duplex DNA increases, while that of the nicked circular DNA decreases. This clearly indicates stand cleavage of the DNA due to singlet oxygen production of **4**. The reactivity of **4** as a singlet oxygen photosensitizer also lasts

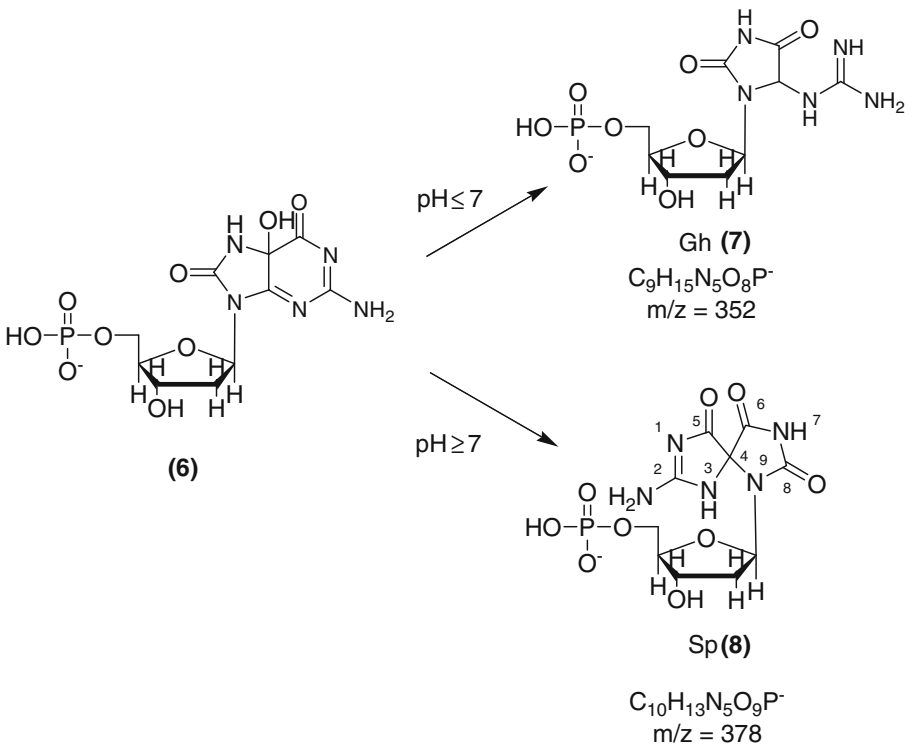

Fig. 10 Oxidation of 5′-dGMP with $[Au^{III}(TMPy_3Pyr_1P)](Cl)_4$ during irradiation at 420 nm. Anaerobic condition: two-electron mechanism and trapping of the $(dGMP\text{-}H)^+$ intermediate to form spiroiminohydantoin 2′-deoxynucleoside 5′-monophosphate (*Sp*). *Gh* guanidinohydantoin 2′-deoxynucleoside 5′-monophosphate

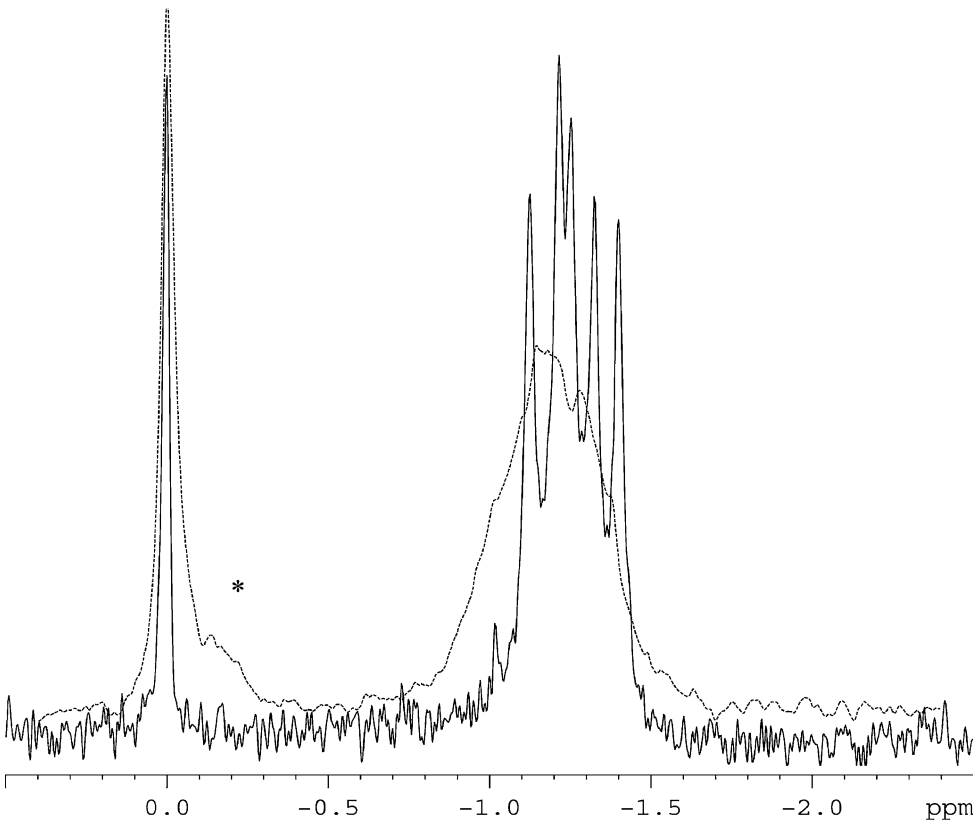

Fig. 11 ^{31}P NMR spectra of free $d(GCGCGC)_2$ B-DNA (*solid line*) and the $d(GCGCGC)_2$ $[Au^{III}(TMPy_3Pyr_1P)](Cl)_4$ complex (*dotted line*) monochromatically irradiated at 420 nm for 2 h under aerobic conditions. 2.5 mM $d(GCGCGC)_2$, 0.16 mM $[Au^{III}(TMPy_3Pyr_1P)](Cl)_4$, 10 mM sodium phosphate, 50 mM NaCl pH 7.0 buffer in 99% D_2O (NMR: 303 K)

for a long period of time because up to 562 min (lane k) conversion of nicked circular DNA to linear duplex DNA is observed on the agarose gel.

Discussion

We have synthesized $[Au^{III}(TMPy_3Pyr_1P)](Cl)_4$ (**4**) and demonstrated that it interacts with A-DNA and B-DNA. The binding of **4** to DNA is significantly different in the case of A-DNA as compared with $H_2(TMPy_3Pyr_1P)(Cl)_4$ (**3**). We have strong indication that the porphyrin ring itself is able to intercalate B-DNA because a negative induced CD band in the Soret region is observed with $d(GCGCGC)_2$. With A-DNA, compounds **3** and **4** show positive and negative induced CD bands in the Soret region of the porphyrin, which is usually interpreted as a sign for outside binding with self-stacking of the porphyrin. But compound **3** shows a negative induced CD band followed by a positive one, while compound **4** shows a positive CD band followed by a negative one. Owing to the pyrenyl moiety of compounds **3** and **4**, these porphyrins have more possibilities to interact with DNA than $H_2(TMPyP)(Cl)_4$. Therefore, we interpret these CD data such that compound **3** has an additional binding mode to A-DNA, which involves the pyrenyl moiety. This is also corroborated by a positive induced CD band at 350 nm with A-DNA. This positive induced CD band was not observed in the spectra of compound **4**. Therefore, we propose that compound **4** interacts with A-DNA and B-DNA similar to the model

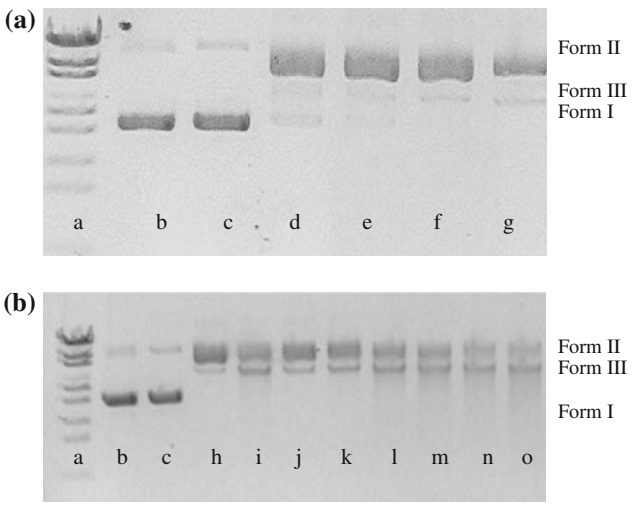

Fig. 12 Photoinduced unwinding and double-strand cleavage of DNA by $[Au^{III}(TMPy_3Pyr_1P)](Cl)_4$. The unwinding of supercoiled pBR322 DNA by $[Au^{III}(TMPy_3Pyr_1P)](Cl)_4$ was determined by agarose gel electrophoresis. *a* DNA marker, *b* 0 min, *c* 10 min, *d* 20 min, *e* 30 min, *f* 40 min, *g* 50 min, *h* 60 min, *i* 120 min, *j* 180 min, *k* 240 min, *l* 320 min, *m* 380 min, *n* 420 min, *o* 480-min irradiation at 420 nm. 0.1 μg μl^{-1} pBR322 DNA, 0.32 mM $[Au^{III}(TMPy_3Pyr_1P)](Cl)_4$, 5 mM sodium phosphate, 75 mM NaCl pH 7.0 buffer

compound H_2(TMPyP)$(Cl)_4$ without any significant additional binding mode using the pyrenyl moiety of **4**. One reason for this could be a slightly different geometry of **4** in comparison with **3**. The melting point experiments with CT-DNA indicate a strong stabilization of the duplex form of CT-DNA by H_2(TMPyP)$(Cl)_4$ and compound **3**. The metalated compounds $[Au^{III}(TMPyP)](Cl)_5$ and **4** showed weaker stabilization than free-base forms of the porphyrins. As a consequence, the complex binding of free-base porphyrins is stronger than that of the metalated ones.

The DPBF assay showed that **4** is able to produce singlet oxygen during irradiation in a Rayonet reactor at 420 nm. The reaction rate is similar to that of the standard rose Bengal. Owing to the fact that **4** is an efficient singlet oxygen producing photosensitizer, it was also able to unwind supercoiled DNA to nicked circular and linear duplex DNA. Therefore, the photosensitizer **4** appears to able to induce strand scission, which is very important for its use as a drug for photodynamic therapy.

The results described above led us to propose a redox mechanism for the photoinduced reaction of **4** with 5′-dGMP or d$(GCGCGC)_2$ duplex DNA under aerobic and anaerobic conditions (Figs. 7, 10). Irradiation at 420 nm under aerobic conditions induces singlet oxygen, which reacts with the guanine base, forming 8-oxo-dGMP (**5**) and 5-HO-8-oxo-dGMP (**6**). Subsequent reactions to **7** and **8**, respectively, could be verified with ^{1}H and ^{13}C NMR spectroscopy and ESI-Q-TOF mass spectrometry (Figs. S1–S3).

The same irradiation procedure under anaerobic conditions leads to the abstraction of one electron from (dGMP-H), producing a radical cationic species $(8\text{-oxo-dGMP})^+$. The attack of a water molecule on $(8\text{-oxo-dGMP})^+$ (also referred to as hydration of the radical cation) produces, after deprotonation of the adduct, a neutral radical species (5-HO-8-oxo-dGMP)·, which can be further oxidized (second electron abstraction) to generate 5-HO-8-oxo-dGMP (**6**). This intermediate collapses into **7** and **8**. Additionally, a degradation product could be identified which was formed by a radical reaction initiated at the C5′ position of the ribose (5′-HO-dGMP). Further oxidation products are obvious but not described.

In summary, **4** is a novel highly water soluble photosensitizer which shows interaction with AT- and GC-rich DNA regions. Owing to its cationic porphyrin backbone, it is supposed that **4** will be accumulated in tumor cells.

In addition to this, **4** shows plasmid DNA cleavage, oligonucleotide cleavage, and guanosine and 5′-dGMP oxidation under aerobic conditions. Even under anaerobic conditions **4** was able to oxidize guanosine and 5′-dGMP. Therefore, **4** has a high potential to be tested on various tumor cell lines in the future. The distinction between the DNA damaging properties evidenced in this paper and the possibility of different cytotoxic effects that might be observed in vitro for the same compound will be the future goal of our research.

Materials and methods

Materials

All materials for synthesis mentioned, CT-DNA, sodium cacodylate, sodium dihydrogen phosphate, disodium hydrogen phosphate, 5′-dGMP, rose Bengal, DPBF, and ethidium bromide, were purchased from Sigma-Aldrich. The oligonucletides d$(GCGCGC)_2$ and d$(ATATAT)_2$ were obtained from MWG Biotech and the plasmid DNA pBR322 was purchased from Fermentas.

Synthesis of the free-base porphyrin

To a refluxing mixture of 50 ml propionic acid and 1 ml propionic anhydride, 1.5 mmol 1-pyrenecarboxaldehyde, 4.5 mmol 4-pyridinecarboxaldehyde, and 6.2 mmol of freshly distilled pyrrole were added. This mixture was refluxed for 90 min. Then the solvent was evaporated to dryness and the black-purple product was dissolved in chloroform. The mixture was divided into several parts and neutralized with a saturated aqueous $NaHCO_3$ solution. The neutralized solution was dried over $MgSO_4$, filtered, and evaporated to dryness. Since this synthesis leads to a mixture of several different *meso*-substituted porphyrins, extensive column chromatography is required to separate the individual porphyrin species. Silica gel was used as a stationary phase and the products were eluted initially with a mixture of chloroform and methanol (19:1, v/v). The different fractions were subjected to column chromatography several times with mixtures of chloroform and methanol in different volume ratios to finally obtain pure compounds. The desired compound, **1** ($R_f = 0.24$), could be identified by mass spectrometry and NMR analysis of each fraction obtained. For further purification, the porphyrin was recrystallized using methanol. The yield was 5% based on the educt 1-pyrenecarboxaldehyde.

^{1}H NMR (500 MHz, $CDCl_3$, 303.57 K, δ, ppm): 9.08 (d, $J = 4.62$, 2H, pyridyl-3,5-H), 9.02 (d, $J = 4.53$, 4H, pyridyl-3,5-H), 8.88 (s, 4H, β-pyrrole-H), 8.78 (d, $J = 7.52$, 1H, pyrenyl-H), 8.72 (d, $J = 4.26$, 2H, β-pyrrole-H), 8.58 (d, $J = 4.26$, 2H, β-pyrrole-H), 8.53 (d, $J = 7.52$, 1H, pyrenyl-H), 8.40 (d, $J = 8.88$, 1H, pyrenyl-H), 8.34 (t, $J = 8.22$, 2H, pyrenyl-H), 8.20 (d, $J = 4.62$, 2H, pyridyl-2,6-H), 8.16 (bs, 4H, pyridyl-2,6-H), 8.08 (m, 2H, pyrenyl-H), 7.70 (d, $J = 9.33$, 1H, pyrenyl-H), 7.38 (d, $J = 9.33$, 1H, pyrenyl-H), −2.64 (s, 2H, pyrrole-NH).

^{13}C NMR (125 MHz, $CDCl_3$, 303.57 K, δ, (ppm): (s = C, d = CH_2, t = CH_3) 162.5 (s, 1C, quart. ipso

pyrenyl-1-C), 150.0 (s, 3C, quart. ipso pyridyl-1-C), 148.6 (d, 2C, pyridyl-3,5-a-CH), 148.5 (d, 4C, pyridyl-3,5-b-CH), 136.2 (s 2C, quart. pyrenyl-C), 133.7 (s, 2C, quart. pyrenyl-C), 132.7 (d, 1C, pyrenyl-CH), 132.7 (d, 2C, β-pyrrole-CH), 131.9 (s, 3C, α-pyrrole-C), 131.9 (s, 3C, α-pyrrole-C), 131.3 (d, 2C, β-pyrrole-CH), 131.2 (d, 4C, β-pyrrole-CH), 130.9 (s, 2C, α-pyrrole-C), 129.5 (d, 2C, pyridyl-2,6-CH), 129.5 (d, 4C, pyridyl-2,6-CH), 128.5 (d, 1C, pyrenyl-CH), 128.1 (d, 1C, pyrenyl-CH), 127.8 (d, 1C, pyrenyl-CH), 126.9 (d, 1C, pyrenyl-CH), 126.6 (d, 1C, pyrenyl-CH), 126.0 (d, 1C, pyrenyl-CH), 125.6 (d, 1C, pyrenyl-CH), 124.7 (s, 1C, quart. pyrenyl-C), 124.3 (s, 1C, quart. pyrenyl-C), 123.0 (d, 1C, pyrenyl-CH), 119.6 (s, 1C, quart. *meso* pyrenyl-C), 117.7 (s, 1C, quart. *meso* pyridyl-a-C), 117.6 (s, 1C, quart. *meso* pyridyl-b-C).

ESI mass spectrometry (chloroform/methanol 1:1, positive ion mode): $m/z = 742.60$ ($[M + H]^+$).

N-alkylation of the porphyrin

To a mixture of 15 ml CH_3NO_2 and 5 ml chloroform (3:1 v/v), 24 μmol **1** and 1.4 mmol methyl *p*-toluenesulfonate were added. This reaction mixture was refluxed for 60 h under an argon atmosphere. The progress of the N-methylation reaction was monitored using silica gel thin-layer chromatography with an eluent containing acetonitrile/H_2O (satuarated KNO_3)/H_2O (8:1:1, v/v). $R_f = 0.32$.

Then the reaction mixture wass evaporated to dryness and dissolved in deionized water and the impurities were extracted with chloroform. The remaining water fraction was filtered and then evaporated to dryness, which gave 5,10,15-tris(*N*-methylpyridinium-4-yl)-20-(1-pyrenyl)-21*H*, 23*H*-porphyrin tosylate (**2**). Yield 93%.

^{1}H NMR (500 MHz, CD_3OD, 303.57 K, δ, ppm): 9.35 (d, $J = 5.48$, 2H, pyridyl-3,5-H), 9.21 (d, $J = 5.45$, 4H, pyridyl-2,6-H), 9.11 (bs, 4H, β-pyrrole-H), 8.91 (d, $J = 5.48$, 2H, pyridyl-3,5-H), 8.73 (bs, 4H, pyridyl-2,6-H), 8.73 (bs, 2H, β-pyrrole-H), 8.50 (d, $J = 7.35$, 1H, pyrenyl-H), 8.50 (bs, 2H, β-pyrrole-H), 8.18 (d, $J = 7.35$, 1H, pyrenyl-H), 8.01 (m, 1H, pyrenyl-H), 7.99 (m, 2H, pyrenyl-H), 7.61 (m, 1H, pyrenyl-H), 7.60 (d, $J = 7.92$, 12H, 3x tosylate-3,5-H), 7.51 (d, $J = 6.67$, 1H, pyrenyl-H), 7.24 (d, $J = 9.20$, 1H, pyrenyl-H), 7.05 (d, $J = 9.20$, 1H, pyrenyl-H), 6.98 (d, $J = 7.92$, 12 H, 3x tosylate-2,6-H), 4.78 (s, 3H, N^+-CH_3), 4.68 (s, 6H, N^+-CH_3), 2.08 (s, 9 H, 3x tosylate CH_3), −2.74 (s, 2H, pyrrole-NH).

^{13}C NMR (125 MHz, CD_3OD, 303.57 K, δ, ppm): (s = C, d = CH_2, t = CH_3) 159.5 (s, 1C, quart. ipso pyrenyl-1-C), 159.3 (s, 3C, quart. ipso pyridyl-1-C), 145.5 (d, 2C, pyridyl-3,5-a-CH), 145.3 (d, 4C, pyridyl-3,5-b-CH), 143.6 (s, 3C, quart. tosylate-1-C), 141.5 (s, 3C, quart. tosylate-4-C), 136.2 (s, 2C, quart. pyrenyl-C), 134.5 (s, 3C, quart. α-pyrrole-C), 134.1 (d, 2C, pyridyl-2,6-CH), 133.9 (d, 4C, pyridyl-2,6-CH) 133.9 (d, 2C, β-pyrrole-CH), 133.5 (d, 1C, pyrenyl-CH), 133.5 (d, 2C, β-pyrrole-CH), 133.2 (d, 4C, β-pyrrole-CH), 133.0 (s, 3C, α-pyrrole-C), 132.6 (s, 2C, α-pyrrole-C), 131.4 (s, 1C, quart. pyrenyl-C), 129.6 (d, 6C, tosylate-2,6-CH), 128.9 (d, 1C, pyrenyl-CH), 128.3 (d, 1C, pyrenyl-CH), 127.3 (d, 1C, pyrenyl-CH), 127.0 (d, 1C, pyrenyl-CH), 127.0 (d, 1C, pyrenyl-CH), 126.8 (d, 6C, tosylate-3,5-CH), 126.2 (d, 1C, pyrenyl-CH), 125.0 (s, 1C, quart. pyrenyl-C), 124.9 (s, 1C, quart. pyrenyl-C), 123.9 (d, 1C, pyrenyl-CH), 122.8 (s, 1C, quart. pyrenyl-1-C), 122.8 (s, 1C, quart *meso* pyrenyl-C), 116.3 (s, 1C, quart. *meso* pyridyl-C), 115.8 (s, 1C, quart. *meso* pyridyl-C), 49.8 (q, 1C, N^+-CH_3), 49.6 (q, 2C, N^+-CH_3), 21.1 (q, 1C, tosylate-CH_3).

ESI mass spectrometry (methanol, positive ion mode): $m/z = 262.20$ ($[M]^{3+}$), $m/z = 392.80$ ($[M]^{2+}$), $m/z = 478.60$ ($[M + tos]^{2+}$).

Ion exchange

Compound **2** (21 μmol) was dissolved in H_2O (35 ml) and methanol (5 ml). Then 2 g of Dowex 1 × 8 Cl^- ion-exchange resin wass added. After 10 h of slow stirring, the ion exchange resin was filtered off and the remaining reaction mixture was evaporated to dryness, which gave **3**. Yield 98%.

Metalation

Compound **3** (6 μmol) and LiCl (40 mg) were dissolved in H_2O (10 ml) and pyridine (300 μl). Then 30 μmol $K[AuCl_4]$ was added, and the reaction mixture was kept at 353 K for 4 h under an argon atmosphere. The progress of the reaction could be monitored by observing the hypsochromic shift of the Soret band of the porphyrin using UV–vis spectroscopy. After the reaction was complete, the mixture was filtered, evaporated to dryness, and the excess of $K[AuCl_4]$ was extracted with acetone. The remaining solid was extracted with methanol and finally gave **4** after evaporation of the solvent. Yield 95%.

^{1}H NMR (500 MHz, CD_3OD, 303.57 K, δ, ppm): 9.62 (q, 4H, β-pyrrole-H), 9.56 (bs, 2H, pyridyl-3,5-H), 9.46 (bs, 4H, pyridyl-3,5-H), 9.42 (bs, 2H, pyridyl-3,5-H), 9.06 (bs, 2H, pyridyl-2,6-H), 9.00 (bs, 2H, pyridyl-2,6-H), 8.97 (m, 4H, β-pyrrole-H), 8.78 (m, 1H, pyrenyl-H), 8.60 (bs, 1H, pyrenyl-H), 8.31 (bs, 1H, pyrenyl-H), 8.21 (bs, 1H, pyrenyl-H), 8.15 (bs, 1H, pyrenyl-H), 7.79 (m, 2H, pyrenyl-H), 7.44 (bs, 1H, pyrenyl-H), 7.09 (bs, 1H, pyrenyl-H), 4.89 (s, 3H, N^+-CH_3), 4.81 (s, 6H, N^+-CH_3).

^{13}C NMR (125 MHz, CD_3OD, 303.57 K, δ, (ppm): (s = C, d = CH_2, t = CH_3) 156.3 (s, 1C, quart. ipso pyrenyl-1-C), 156.2 (3C, quart. ipso-pyridyl-1-C), 146.9 (4C, pyridyl-3,5-a,c-CH), 146.4 (d, 2C, pyridyl-3,5-b-CH),

139.9 (s, 2C, quart α-pyrrole-C), 137.3 (s, 2C, quart α-pyrrole-C), 137.1 (s, 2C, quart α-pyrrole-C), 137.0 (s, 2C, quart α-pyrrole-C), 135.0 (d, 2C, pyridyl-2,6-a-CH), 134.6 (s, 1C, quart. pyrenyl-C), 134.3 (d, 4C, β-pyrrole-CH), 134.1 (d, 4C, β-pyrrole-CH), 133.9 (d, 2C, pyridyl-2,6-c-CH), 133.7 (d, 2C, pyridyl-2,6-b-CH), 133.7 (d, 1C, pyrenyl-CH), 133.4 (s, 1C, quart. pyrenyl-C), 132.6 (s, 1C, quart. pyrenyl-C), 131.3 (s, 1C, quart. pyrenyl-C), 130.8 (d, 1C, pyrenyl-CH), 130.5 (d, 1C, pyrenyl-CH), 129.6 (d, 1C, pyrenyl-CH), 127.6 (d, 2C, pyrenyl-CH), 127.6 (d, 1C, pyrenyl-CH), 126.9 (d, 1C, pyridyl-CH), 125.1 (s, 1C, quart. pyrenyl-C), 124.9 (s, 1C, quart. pyrenyl-C), 124.8 (s, 1C, quart. ipso pyrenyl-1-C), 124.6 (d, 1C, pyrenyl-CH), 119.1 (s, 2C, *meso* pyridyl-a,c-C), 118.8 (s, 1C, *meso* pyridyl-b-C), 49.9 (q, 3C, N^+-CH_3).

High-resolution ESI-Q-TOF (methanol, positive ion mode): $m/z = 245.3201$ ($[Men]^{4+}$).

Photolysis reactions of **4** with 5′-dGMP, guanosine, and d(GCGCGC)$_2$ B-DNA

Visible-light irradiation of photosensitizer **4** in the presence of dGMP, guanosine, and B-DNA d(GCGCGC)$_2$ was carried out in buffered aqueous solutions at ambient temperature in a Rayonet photoreactor (Southern New England UV, model RPR-100) equipped with eight RPR-4190 fluorescent tube lamps emitting in the blue spectral region between 400 and 450 nm with a maximum output around 420 nm (abouit 25 mW cm^{-2} of irradiance at the surface). An approximate illuminance of 3,100 ± 100 lux was measured at the sample position (about 10-cm distance) with a cosine-corrected digital light meter (Reliability Direct AR823).

Reaction preparation

Guanosine degradation

Degradation was achieved by irradiation (RPR-4190) of 0.08 mM guanosine with 0.05 mM **4** in 5 mM sodium phosphate buffer at pH 7.0 containing 75 mM NaCl under aerobic and anaerobic conditions.

Singlet oxygen assay

Photosensitized singlet oxygen generation by rose Bengal (0.05 μM) and **4** (0.03 mM) was monitored in aerobic ethanol solution at 298 K by following the time-dependent spectral variations at 410 nm in the presence of DPBF acting as a $^1O_2$ scavenger [68]. The absorbance of the main Q-band maximum of **4** and the absorption maximum of rose Bengal were set to approximately identical values. Samples were irradiated with the full light of a high-pressure mercury lamp passing through a Schott GG 495 nm cutoff filter. As a control, no bleaching of DPBF occurred under anaerobic irradiation conditions. The absolute singlet oxygen ($^1\Delta_g$) quantum yield of the reference standard rose Bengal is reported as $\phi_\Delta = 0.68$ in ethanol [69].

Plasmid degradation

A solution of plasmid DNA (0.1 μg μl^{-1} pBR322 DNA) and 0.32 mM **4** solution in 5 mM sodium phosphate pH 7.0 buffer was prepared for the photodegradation experiments.

Oligonucleotide degradation

The photooxidation process was carried out under aerobic conditions on 2.5 mM d(GCGCGC)$_2$ duplex DNA solutions. The porphyrin concentration was 0.16 mM **4**, and the solutions were buffered to pH 7.0 with a 10 mM sodium phosphate solution in 99% D_2O.

Photooxidation of 5′-dGMP and guanosine

The photoinduced reaction of 5′-dGMP and guanine with **4** was investigated under aerobic and anaerobic conditions with a 5.0 mM 5′d-GMP solution and 10 μM **4** in 99% D_2O and 1.65 mM guanosine and 0.16 mM **4** in 5 mM sodium phosphate, 75 mM NaCl pH 7.0 buffer in 99% D_2O, respectively. Monochromatic irradiation was carried out in Teflon-stoppered 1-cm quartz spectrophotometer cells on an optical bench equipped with a Hanovia xenon/mercury 977 B1 (1-kW) lamp, a Schoeffel GM 250-1 monochromator, and a quartz condenser.

NMR spectroscopy

NMR spectra were recorded using Bruker NMR spectrometer equipped with a broadband inverse tunable probe operating at 200 MHz for ^{1}H and 80.961 MHz for ^{31}P. Additionally, higher-resolved ^{1}H and ^{13}C spectra were recorded using a Bruker NMR spectrometer operating at 500 MHz for ^{1}H and 125.725 MHz for ^{13}C. Chemical shifts for ^{1}H and ^{31}P are reported relative to tetramethylsilane and 85% H_3PO_4, respectively, each at 0.00 ppm. Samples were prepared in D_2O and the residual water signal was further suppressed with a presaturation, and to obtain information on H1′ protons separate experiments were performed using a watergate pulse sequence. Photo-time-course reactions were followed by NMR experiments at 303 K recording spectra at 1-h intervals. ^{1}H spectra were recorded using 1,024 scans and ^{31}P NMR spectra were obtained using 10,240 scans with ^{1}H broadband decoupling.

ESI mass spectrometry

Mass spectra were collected using a Finnigan LCQ Deca-XPplus ion trap mass spectrometer with an ESI ion source and an Agilent ESI-Q-TOF 6250 instrument. The various porphyrin samples were dissolved in chloroform/methanol (1:1) or methanol. Then they are introduced to the mass spectrometer via infusion at a flow rate of 0.30 ml h^{-1}. The source and desolvation temperatures were 353 and 393 K, respectively. The capillary voltage was set to 3.1 kV, the sampling cone voltage to 58 V, and the extractor cone to 3 V. The collision energy was set to 14 eV. Argon, used as a collision gas for the collision-induced-dissociation experiments, was adjusted to a pressure of 1.7×10^{-4} mbar.

UV absorption

UV-absorption spectra of a 0.1 μM **4** solution and a 0.1 μM **4** solution in 5 mM sodium cacodylate, 20 mM NaCl pH 7.0 buffer were obtained with a Varian CARY 100 Bio UV–vis spectrometer equipped with Cary temperature controller.

Circular dichroism

CD spectra of the DNA porphyrin/oligonucleotide complexes were all recorded with a JASCO J-810 spectropolarimeter equipped with JASCO PTC-423S temperature controller on equimolar 0.2 mM $d(GCGCGC)_2$/$d(ATATAT)_2$, 0.2 mM **4** solutions in 5 mM sodium cacodylate, 20 mM NaCl pH 7.0 buffer (293 and 278 K).

Cyclic voltammetry

All electrochemical experiments were carried out under an inert atmosphere in a glove box (UNILab, M. Braun) using a home-built cylindrical three-electrode cell equipped with vacuum-tight fittings and spiral-shaped platinum and silver wires as the counter and pseudo-reference electrodes. A platinum disk working electrode (BAS, 1.6 mm), freshly polished with 1-μm diamond slurry, was used for all measurements. Cyclic voltammogramms were recorded with a computer-controlled Autolab PGSTAT 20 electrochemical workstation (Eco-Chemie), applying scan rates in the range 50–200 mV s^{-1} at room temperature. The sample materials were dissolved in deoxygenated *N*,*N*′-dimethylformamide with 0.1 M NBu_4PF_6 (electrochemical grade, Fluka) as the supporting electrolyte. Ferrocene was added as an internal standard for potential calibration.

Emission spectra and luminescence lifetimes

Samples of **4** were measured in 99% ethanol glass at 77 K. The emission and lifetime measurements were obtained using a Horiba Jobin Yvon Fluorolog-3 spectrofluorometer equipped with two double-grating monochromators, a R928P photomultiplier, and an FL-1040 phosphorimeter. The low-temperature spectra were recorded with a liquid nitrogen filled Dewar accessory containing a Pyrex sample holder. All emission spectra were corrected for wavelength-dependent instrument and detector response. Luminescence lifetimes were measured at 77 K with a pulsed UV xenon flash tube using the R928P detector in the photon-counting mode with a variable delay and an open window between the pulse and detection. The samples were excited in the Soret-band region at 408 nm, with 41 flashes measured per scan. For the measurement of time-gated luminescence spectra, the integration time was 20 μs and a 50-μs delay between the excitations was employed.

Acknowledgments W.S. acknowledges the support of the Austrian Science Fund FWF (P-18384—Solid state and liquid NMR of biomolecular metal complexes) and the financial support of the European Community (EU-NMR, contract no. RII3-026145). W.S. also acknowledges the help of Klaus Wolkenstein and Clemens Schwarzinger for ESI-Q-TOF mass spectrometry and matrix-assisted laser desorption/ionization TOF mass spectrometry measurements. G.K. acknowledges the support by the DFG Graduate College 640 "Sensory photoreceptors in natural and artificial systems."

References

1. Gray HB, Stiefel EI, Valentine JS, Bertini I (eds) (2007) Biological inorganic chemistry: structure and reactivity. University Science Books US, p 739
2. Bolster MW (1997) Pure Appl Chem 69
3. Knör G (2009) Chem Eur J 15:568–578
4. Kirsch-De Mesmaeker A, Puerard F (2006) Inorg Chem Commun 9:111–126
5. Armitage B (1998) Chem Rev 98:1171–1200
6. Eng MP, Ljungdahl T, Andréasson J, Mårtensson J, Albinsson B (2005) J Phys Chem A 109:1176–1784
7. Knör G (2001) Inorg Chem Commun 4:160–163
8. Schoefberger W, Haeubl M, Schürz S, Svejda B, Pfragner R, Müller N, Patent E (eds) (2009) p 80
9. Yam VW-W, Cheng EC-C (2007) Top Curr Chem 281:269–309
10. Sies H (1991) Oxidative stress: oxidants and antioxidants. Academic Press, London
11. Marnett LJ, Burcham PC (1993) Chem Res Toxicol 6:771–785
12. Cadet J (1994) IARC scientific publication no 125. IARC, Lyons, pp 245–276
13. Burrows CJ, Muller JG (1998) Chem Rev 98:1109–1151
14. Pyle AM, Barton JK (1990) Prog Inorg Chem Bioinorg Chem 38:413–475
15. Chow CS, Barton JK (1992) Methods Enzymol 212:219–242
16. Lutterman DA, Fu PK-L, Turro C (2006) J Am Chem Soc 128:738–739

17. Aguirre JD, Lutterman DA, Angeles-Boza AM, Dunbar KR, Turro C (2007) Inorg Chem 46:7494–7502
18. Vialas C, Pratviel G, Claparols C, Meunier B (1998) J Am Chem Soc 120:11548–11553
19. Chworos AC, Coppel Y, Dubey I, Pratviel G, Meunier B (2001) J Am Chem Soc 123:5867–5877
20. Clarke MJ, Morrissey PE (1984) Inorg Chim Acta 80:L69–L70
21. Gariepy KC, Curtin MA, Clarke MJ (1989) J Am Chem Soc 111:4947–4952
22. Farrer BT, Thorp HH (2000) Inorg Chem 39:44–49
23. Carter PJ, Cheng CC, Thorp HH (1998) J Am Chem Soc 120:632–642
24. Carter CP, Cheng C-C, Thorp HH (1996) Inorg Chem 35:3348–3354
25. Cheng C-C, Goll JG, Neyhart GA, Welch TW, Singh SP, Thorp HH (1995) J Am Chem Soc 117:2970–2980
26. Muller JG, Kayser LA, Paikoff SJ, Duarte V, Tang N, Perez RJ, Rokita SE, Burrows CJ (1999) Coord Chem Rev 185–186:761–774
27. Burrows CJ, Perez RJ, Muller JG, Rokita SE (1998) Pure Appl Chem 70:275–278
28. Muller JG, Duarte V, Hickerson RP, Burrows CJ (1998) Nucleic Acids Res 26:2247–2249
29. Reedijk J (1996) Chem Commun (7):801–806
30. Takahara PM, Rosenzweig AC, Frederick CA, Lippard SJ (1995) Nature 377:649–651
31. Ohndorf U-M, Rould MA, He Q, Pabo CO, Lippard SJ (1999) Nature 399:708–712
32. Hall MD, Hambley TW (2002) Coord Chem Rev 232:49–67
33. Hartley FR (1991) Elsevier, Amsterdam
34. Novakova O, Vrana O, Kiseleva VI, Brabec V (1995) Eur J Biochem 228
35. Talman EG, Kidani Y, Mohrmann L, Reedijk J (1998) Inorg Chim Acta 283:251–255
36. Galanski M, Keppler BK (2000) Inorg Chim Acta 300–302:783–789
37. Choi S, Filotto C, Bisanzo M, Delaney S, Lagasee D, Whitworth JL, Jusko A, Li C, Wood NA, Willingham J, Schwenker A, Spaulding K (1998) Inorg Chem 37:2500–2504
38. Choi S, Mahalingaiah S, Delaney S, Neale NR, Masood S (1999) Inorg Chem 38:1800–1805
39. Choi S, Orbai L, Padgett EJ, Delaney S, Hakemian AS (2001) Inorg Chem 40:5481–5482
40. Puddephatt RJ (1978) Elsevier, Amsterdam
41. Buckley RG, Elsome AM, Fricker SP, Henderson GR, Theobald BR, Parish RV, Howe BP, Kelland LR (1996) J Med Chem 39:5208
42. Gabbiani C, Casini A, Messori L (2006) Gold Bull 40:73–81
43. Coronnello M, Mini E, Caciagli B, Cinellu MA, Bindoli A, Gabbiani C, Messori L (2005) J Med Chem 48:6761
44. Ronconi L, Giovagnini L, Marzano C, Bettio F, Graziani R, Pilloni G, Fregona D (2005) Inorg Chem 44:1867–1881
45. Che C-M, Sun RW-Y, Yu WY, Ko CB, Zhu N, Sun H (2003) Chem Commun 1718–1719
46. Fleischer EB, Laszlo A (1969) Inorg Nucl Chem Letts 5:373
47. Tiekink ERT (2008) Inflammopharmacology 16:138–142
48. Rigobello MP, Scutari G, Folda A, Bindoli A (2004) Biochem Pharmacol 67:689
49. Omata Y, Folan M, Shaw M, Messer RL, Lockwood PE, Hobbs D, Bouillaguet S, Sano H, Lewis JB, Wataha JC (2006) Toxicol In Vitro 20:882–890
50. Hurley LH (2002) Nat Rev Cancer 2:188
51. Lipscomb LA, Zhou FX, Presnell SR, Woo RJ, Peek ME, Plaskon RR, Williams LD (1996) Biochemistry 35:2818
52. Hengartner MO (2000) Nature 407:770
53. Hunt A, Evan G (2001) Science 293:1784
54. Sun RW-Y, Yu W-Y, Sun H, Che C-M (2004) Chem Biochem 5:1293–1298
55. Lum CT, Yang ZF, Li HY, Sun RW-Y, Fan ST, Poon RTP, Lin MCM, Che C-M, Kung HF (2006) Int J Cancer 118:1527–1538
56. Wang Y, He Q-Y, Che C-M, Chiu J-F (2006) Proteomics 6:131–142
57. Eng M, Ljungdahl T, Andrasson J, Mrtensson J, Albinsson B (2005) J Phys Chem A 109:1776–1784
58. Kadish KM, EW, Ou Z, Shao J, Sintic PJ, Ohkubo K, Fukuzumi S, Crossley MJ (2002) Chem Commun 356–357
59. Guliaev AB, Leontis NB (1999) Biochemistry 38:15425–15437
60. Kim JO, Lee Y-A, Yun BH, Han SW, Kwag ST, Kim SK (2004) Biophys J 86:1012–1017
61. Pasternack RF, Gibbs EJ (1993) J Inorg Organomet Polym 3:77–88
62. Marzilli LG (1990) New J Chem 14:409–420
63. Fiel RJ (1989) J Biomol Struct Dyn 6:1259–1274
64. Ravanat J-L, Saint-Pierre C, Mascio PD, Martinez GR, Medeiros MHG, Cadet J (2001) Helv Chim Acta 84:3702–3709
65. Ravanat J, Di Mascio P, Martinez GR, Medeiros MHG (2000) Cadet J 275:40601–40604
66. Pratviel G, Meunier B (2006) Chem Eur J 12:6018–6030
67. Torun L, Morrison H (2003) Photochem Photobiol 77:370–375
68. Packer L, Sies H (2000) Singlet oxygen, UV-A and ozone. Academic Press, San Diego
69. Wilkinson F, Helman WP, Ross AB (1993) J Phys Chem Ref Data 22:113–262